The electronic structure of transition metal interacting tip and sample and atomic force microscopy. II

1995 J. Phys.: Condens. Matter 7 6641

(http://iopscience.iop.org/0953-8984/7/33/005)

J. Phys.: Condens. Matter 7 (1995) 6641–6661. Printed in the UK

The electronic structure of transition metal interacting tip and sample and atomic force microscopy—part II

H Ness† and F Gautier‡

† Department of Physics, University of Durham, South Road, Durham DH1 3LE, UK
‡ IPCMS–GEMME, Bâtiment 69, 23 rue du Loess, 67037 Strasbourg, France

Received 18 May 1995

Abstract. A detailed theoretical study of the interaction of transition metal nanotips with surfaces is performed in the tight-binding scheme. The real space recursion method is used to determine the local densities of states (LDOS) of the interacting tips and samples. We consider more especially W supported pyramidal tips with different morphologies. The interaction of W supported tips with W(001) surfaces is studied within the intermediate-interaction regime for which metallic adhesive forces are dominant. The electronic structure of both the tip and the sample are found to be substantially modified due to the tip/sample (T/S) interaction. The T/S interaction energy curves are also calculated when the tip's apex is located above high-symmetry surface sites. It is shown that the T/S interaction energy can be reproduced with a good accuracy using the model of a square LDOS. Finally, we present a simple numerical scheme to obtain atomic force images. We study the influence of the tip's morphology and of the surface's defects on the contrast of the resulting images.

1. Introduction

In the first part of this study [1], we investigated the electronic structure of both supported nanotips and cluster tips with different morophologies. We have shown that the electronic structure of supported tips is quite different from the one of the corresponding cluster tips. This is an important feature when the tunnelling current between the tip and the sample is calculated from perturbation-type theory [2–5]. In this paper we assess another important point for the understanding of images obtained by scanning tunnelling microscopy (STM) and atomic force microscopy (AFM). This point concerns the importance of the modifications of the electronic structure of the tip and of the sample when both systems interact 'strongly'. Let us first summarize our present knowledge of theoretical models for STM and AFM in relation to the importance of the tip/sample (T/S) interaction and of the tip's morphology (subsections 1.1 and 1.2). Then we present the goal of the present study and the summary of this paper (subsection 1.3).

1.1. Tip/sample interaction and scanning tunnelling microscopy

When the T/S distance d is small (d = 2–5 Å), it is necessary to go beyond the Bardeen perturbation approximation [2, 3] in order to take account of the coupling between the tip and sample states. For example, Sacks and Noguera have developed a generalized expression for the tunnelling current [6]. The difference of their expression from the Tersoff and Hamann formula [3] lies especially in the presence of a renormalization factor that takes

0953-8984/95/336641+21$19.50

into account the modifications of the surface LDOS due to the presence of the tip. These modifications are important in the case of 'strong' T/S coupling and more especially when the combination of tip and sample states leads to tip-induced localized states (TILS) as previously noticed by Ciraci *et al* [7, 8].

Another model, proposed by Doyen *et al* [9], takes also into account 'strong' T/S coupling. However for numerical simplicity, the tip is modelled by a single atom deposited on a perfect surface. Such calculations allow us for example to show that the 'strong' coupling between the tip and the sample can introduce an inversion of the contrast in the images of Pd surfaces. They show that the STM images can be strongly modified by the close proximity of the tip, the tip electronic structure playing a very important role in the tunnelling process. Therefore, a detailed theoretical study of nanotip-like electronic structure and of the modifications of the electronic structures of such tips and samples due to their interaction is much needed.

1.2. Atomic force microscopy and T/S interaction models

The AFM [10, 11] allows us to visualize both conducting and non-conducting surfaces at the atomic scale. Atomic resolution has been achieved on layered materials [12–14], on ionic crystals [15] and also on metallic surfaces [16]. It has been shown that the atomic resolution and the observed corrugation are strongly dependent on the value of the force involved during the experiment (i.e. on the value of the T/S distance d) and on the unknown tip morphology. Therefore it is necessary to know the nature of the forces involved during the experiments and to understand the influence of the tip morphology on the images. Different interaction regimes we briefly discuss now can be defined according to the T/S separation.

At large distances ($d \gtrsim 10$ Å), the interaction is dominated by attractive forces of the Van der Waals type. Such pair interaction forces are small for each individual contribution but the resulting T/S forces are sizable because they result from the superposition of a huge number of these pair contributions originating from the tip. At small distances ($d < 1$ Å), short-range forces arising from the strong overlap between the tip and sample electronic densities are the most important. They are strongly repulsive and are easily measured. Most of the experimental images have been obtained within this regime. However, these forces lead to strong deformations of the T/S junction which are irreversible so the interpretation of the images becomes difficult.

In the intermediate regime between the above two 'extreme' cases, the deformations of both the tip and the sample are thought to be relatively small. Such an intermediate regime has been extensively studied by Dürig *et al* for metallic tips and samples using both STM and AFM [11, 17]. They have shown that the observed forces are consistent with short-range metallic adhesive forces which determine the AFM contrast. Such short-range forces can be measured for T/S distances larger than those for which electrical and mechanical contacts successively occur between the tip and the sample. Furthermore these authors also have shown that in this intermediate regime the contribution (over the whole tip) of the Van der Waals forces to the T/S force gradient is negligible [17]. Consequently, the long-range Van der Waals forces do not modify drastically the contrast induced by the adhesive forces at the atomic scale.

On the other hand, the influence of the tip's morphology on the images (i.e. the loss of the atomic resolution, the distortion of the images, ...) has been proved experimentally. Therefore a detailed theoretical study of the contrast and of its dependence upon the tip morphology is also needed. However, up to now, few theoretical calculations concerning

the AFM have been achieved, the tip being usually modelled in a very simple way. For example, using *ab initio* calculations, Zhong *et al* modelled a Pd sharp tip by a single atom in order to study the AFM corrugation of graphite surfaces [18]. Ciraci *et al* have studied the forces and deformations of a single Al atom tip deposited on an Al surface and interacting with another perfect Al surface [19]. Ciraci *et al* have also performed a study of the short- and long-range forces between an Al blunt tip and an Al sample [20], the blunt tip they consider being modelled by another slab facing the surface.

For more complex tip structures, semiempirical methods have been used. For example Abraham *et al* have considered tips made of one to four Si atoms interacting with an Si surface via empirical potentials (pair and triplet interaction potentials) [21]. They have studied the influence of the tip's morphology on the AFM images they obtained. Tekman and Ciraci used a periodic force field to model Al blunt tips—(4×4) or (5×5) flake—interacting with Al or graphite surfaces [22]. They considered more especially the repulsive force regime and showed that the image distortions are clearly related to the tip's morphology. Bozzolo and Ferrante used a modified equivalent crystal theory to describe the bimetallic interaction between a sample and tips made up of one to five atoms [23]. They showed the influence of the chemical nature of the tips and sample on the corresponding T/S forces.

Finally some calculations have been performed in the molecular dynamics framework to take account of the deformations induced by the T/S interaction. These calculations are based on semiempirical models for the electronic structure. They are more especially devoted to the study of the indentation processes. Different metallic systems have been considered. For example Landman *et al* studied adhesion, nanoindentation and fracture at the atomic scale for Ni tips and Au samples [25] within the framework of the embedded atom method; Sutton *et al* studied the mechanical properties of Ir (Pb) tip and Ir (Pb) sample [25] using the Finnis–Sinclair empirical potentials. These calculations show that during the indentation process both strong T and (or) S irreversible deformations and atomic flows from the S to the T (or *vice versa*) occur. They are strongly dependent upon the mechanical properties of the considered systems and are much smaller for hard materials such as transition metals (W, Ir, Re, ...) than for soft metals (Pb for example) [25].

1.3. Summary

The purpose of this paper is to evaluate the modifications of the electronic structure of both the tip and the sample surface when they are put close to each other. The T/S interaction energies and the influence of the tip morphology on these interaction energies and on the corresponding forces are also obtained. The regime of T/S separations we consider here is the intermediate-interaction regime ($d = 2$–5 Å) where the tip/sample orbitals' overlap is sufficient to create T/S 'chemical bonds'. This regime is similar to the one considered by Sacks and Noguera [6], Ciraci *et al* [8] and Dürig *et al* [17]. In this intermediate regime, the adhesive forces determine the AFM contrast, the short-range repulsive forces ($d < 1$ Å) and the long-range Van der Waals forces being of smaller importance.

The tips are assumed to be pyramids whose apexes are of atomic dimensions. Tips having the same shape as those obtained experimentally by Vu Thien Binh *et al* [26] are also considered. We restrict the present study to the transition metal W tips and samples. The interaction of these tips with W surfaces and the modifications of both the tip and sample surface LDOS are studied, as well as the evolution of the T/S interaction energy. The geometrical complexity of such systems involves supercells too large for *ab initio* calculations and hence computing times too large to determine the band structure of these systems. This is why we choose the tight-binding approach to describe the electronic

structure of the considered systems. We also use the real space recursion method to calculate the LDOS of the T/S systems.

The content of the paper is as follows. In section 2 we briefly present the method of calculation. In section 3, we discuss the modifications of the tip and sample LDOS due to their interaction. Section 4 is devoted to the general properties of the T/S interaction energy and to the range of validity of scaling laws. Using further approximations for the energy, we develop a simple numerical scheme to obtain AFM images (section 5). This will allow us to establish precisely the conditions to obtain atomic resolution in the attractive adhesive force range. We study more especially the influence of the tip's morphology and of the surface's defects on the atomic force contrast. Finally we summarize the most significant results we have obtained (section 6).

2. Method of calculation

The method of calculation and the model for the energy have already been described in more detail in the first part of the study [1]. Let us now briefly recall the salient features of such a method.

2.1. Model for the energy

The total energy $E = E_{bs} + E_r$ results from two contributions. The repulsive energy E_r is chosen to be described by a pair potential of the Born–Mayer type whose parameters are fitted to obtain the bulk isotropic compressibility B_c and cohesive energy E_c. Then the calculated equilibrium lattice parameter a_0 is nearly equal to the experimental one. The values we have chosen for W [27] are close to those of Gschneidner [28]. The attractive band term E_{bs} is obtained from the LDOS. In this first study, the energy E_{bs} is the one-electron contribution due to the 'd' electrons of the considered transition metal. The tight-binding Hamiltonian is obtained from the energy levels $\varepsilon_{i\lambda}$ and the hopping integrals $t_{\lambda\mu}(\boldsymbol{R}_{ij})$ between two sites i and j (λ and μ label the different orbital symmetries). The hopping integrals are described by a linear combination of the three Slater–Koster parameters ddσ, ddπ, ddδ [29]. These parameters are assumed to vary exponentially with the interatomic distance. They are non-zero only between first- and second-nearest neighbours (NN). For the study of the T/S interaction forces, we must perform an analytical continuation for the hopping integrals to avoid artificial discontinuities in the numerical calculation of the forces. In this case, the $t(R)$ have been chosen to decrease continuously to zero with interatomic distance R when $R_p < R < R_c$ ($R_c = R_3$ is the interatomic cut-off distance) with R_p, the value for which the analytical continuation begins, lying between R_2 and R_3 (R_n being the equilibrium distance between two nth NN). We have also tried different forms for the continuation or for the analytical forms for the hopping integrals. As we have already mentioned, the results we obtain for such different distance dependences do not significantly modify the LDOS either for the atoms of the sample surfaces or for those of the tips [1].

In our calculations, we required self-consistent local neutrality on each atomic site. The self-consistent procedure is performed assuming that the local energy levels $\varepsilon_{i\lambda}$ are independent of the considered 'd' orbital symmetry ($\varepsilon_{i\lambda} = \varepsilon_i$). These levels are determined to obtain the band filling within the local neutrality with an accuracy of 10^{-4}. In practice, this self-consistent procedure is performed for the tip atoms and for the three first planes of the sample (S) and of the tip's support (TSp) from their respective surfaces, with a lateral extent limited to the equivalent of twice the tip's basal area. This cut-off defines the 'perturbation domain' (containing up to 50 inequivalent atoms when the tip is located

at high-symmetry surface sites). Its choice results from the fact that the energy levels and electronic structures of the free semi-infinite S and TSp metals are recovered at the boundaries of this domain.

Finally in this scheme, the band structure energy may be written as a sum of local energies E_i^{bs} over all the atoms constituting the system as mentioned in the first part of this study [1].

2.2. The calculation of the densities of states

The LDOS are calculated by the recursion method [30] with N exact pairs of recursion coefficients (a_n, b_n). The asymptotic values (a_∞, b_∞) are obtained by the Beer–Pettifor method [31], which determines the exact value of the centre of the spectral support (a_∞) and the exact value of the spectral support's width $(4\sqrt{b_\infty})$ for the considered state.

For most of the cases we consider here, we have found that the value $N = 8$ represents a satisfactory compromise between precision and computing time. However note that when the tip and sample are chosen to be of different chemical species there may be a peculiar behaviour of the coefficients. This behaviour originates from the differences of the band width and band filling between atoms of different chemical natures. In fact, the spectral support of the $|i\lambda\rangle$ state can be considered as the 'union' of the spectral supports of all the atoms encountered in the calculation of the iterative recursion base. Finally, the calculated spectral support of the $|i\lambda\rangle$ state can be substantially larger than that of the corresponding bulk state, because of the different energy positions of the spectral supports for all the considered atoms. This is why we observe in such a case a crossover between two regimes corresponding to low and high values of the b_n coefficients. In such cases, the asymptotic regime is obtained for larger values of N (for example, $N = 14$ for the case of an Fe tip and an Ni sample).

2.3. The structure of the considered systems

The perfect tips are assumed to be the sharpest possible perfect pyramids (pyr) with a monoatomic apex and are supported by a perfect semi-infinite bcc crystal (TSp). They are built from h perfect bcc (001) or (111) planes. We also considered truncated pyramids (tpyr). They are obtained from the perfect ones when suppressing the topmost atoms, so that they have multiatomic apexes with for example four or nine atoms for (001) planes and three or six for (111) planes. The sample is also assumed to be a perfect semi-infinite bcc crystal, limited by a (001) or (111) surface with or without steps. The z axis is chosen to be perpendicular to the (001) surface. (See for example figure 1.)

Finally as a first step for such calculations, the interacting tip and sample are separated rigidly without surface relaxation, reconstruction or tip or sample deformations from their interaction. The distance d between the apex and the surface is assumed to vary between one and three interplanar distances $d_{(hkl)}$ (with $(hkl) = (001)$ or (111)). The approximation of a rigid tip and sample seems *a priori* to be rather crude, but we guess that we can obtain good trends concerning the tip electronic structure and the T/S interaction and quite good qualitative features for the contrast of AFM images. Of course this model cannot describe the extreme cases for which (i) there is a snapping together of the tip and sample [32] or (ii) there are irreversible deformations of the sample and (or) the tip (strong-repulsive-force regime). In order to clarify this point and to estimate the range of the T/S distances for which the above approximations are still valid, preliminary tight-binding molecular dynamics calculations have been performed. They have shown, for example, that for hard

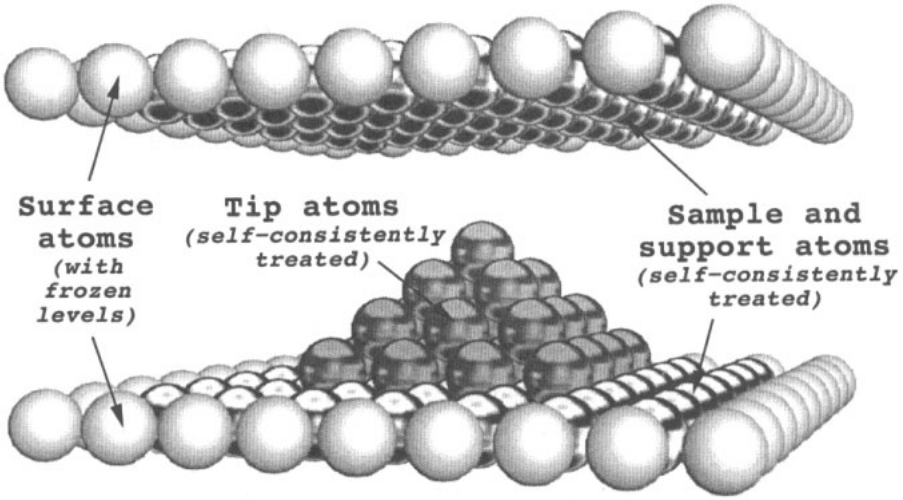

Figure 1. A schematic three-dimensional representation of the supported pyr(001) $h = 4$ tip interacting with a (001) sample surface. The 'perturbation domain' is defined by the tip and sample atoms which are labelled to be 'self-consistently' treated. Note that only a limited extent of the tip's support and of the sample surface are shown.

materials such as Re, the deformations of the tip and sample are not drastically important for the regime of attractive adhesive T/S forces we consider here [33]. Similar behaviours have been obtained for hard-transition-metal T/S systems (such as Ir) [25].

3. T/S interaction—LDOS modifications

In this section, we study the interaction between the perfect W supported tip pyr(001) $h = 4$ and a W(001) surface (S) versus d (d is the distance between the sample surface and the tip apex). We assume that the apex occupies either a hollow (H) site (i.e. a site above the centre of a square of first surface NN) or a top (T) site (i.e. a site on top of a sample's surface atom).

First we discuss the modifications of the apex LDOS and of its NN on the sample surface (sNN). As the T/S distance d decreases, the number of NN of the apex and of the sNN atoms increases. Hence, the corresponding LDOS broadens progressively. This broadening is less important for a T site, because there are fewer bonds between the tip and the sample than for an H site. The aLDOS and the sNN LDOS present new structures introduced by the tip and sample atoms which interact directly via large hopping integrals. For example, with a pyn(001) $h = 4$ facing an H site, the qualitative bonding and antibonding features of the aLDOS are more and more marked for decreasing values of d (figure 2(a)); the states above and below ε_F are progressively shifted towards the top and bottom of the band respectively. These shifts induced a strong hole in the middle of the aLDOS. This hole is directly related to the decrease of the W(001) surface peak in the sNN LDOS (figure 2(a)), which nearly disappears for $d/d_{(001)} < 1$. With a pyn(001) $h = 4$ facing a T site, a new peak appears above ε_F in the aLDOS (figure 2(b)). While the qualitative bonding and antibonding features decrease slowly for decreasing d values, this new peak is shifted towards high energies with an increasing amplitude. This peak is due to the strong interaction between the apex and its on-top sNN. It corresponds to a strong d_{z^2}-directed bond. Note that for $d/d_{(001)} = 2$, the apex and its unique sNN are second NN.

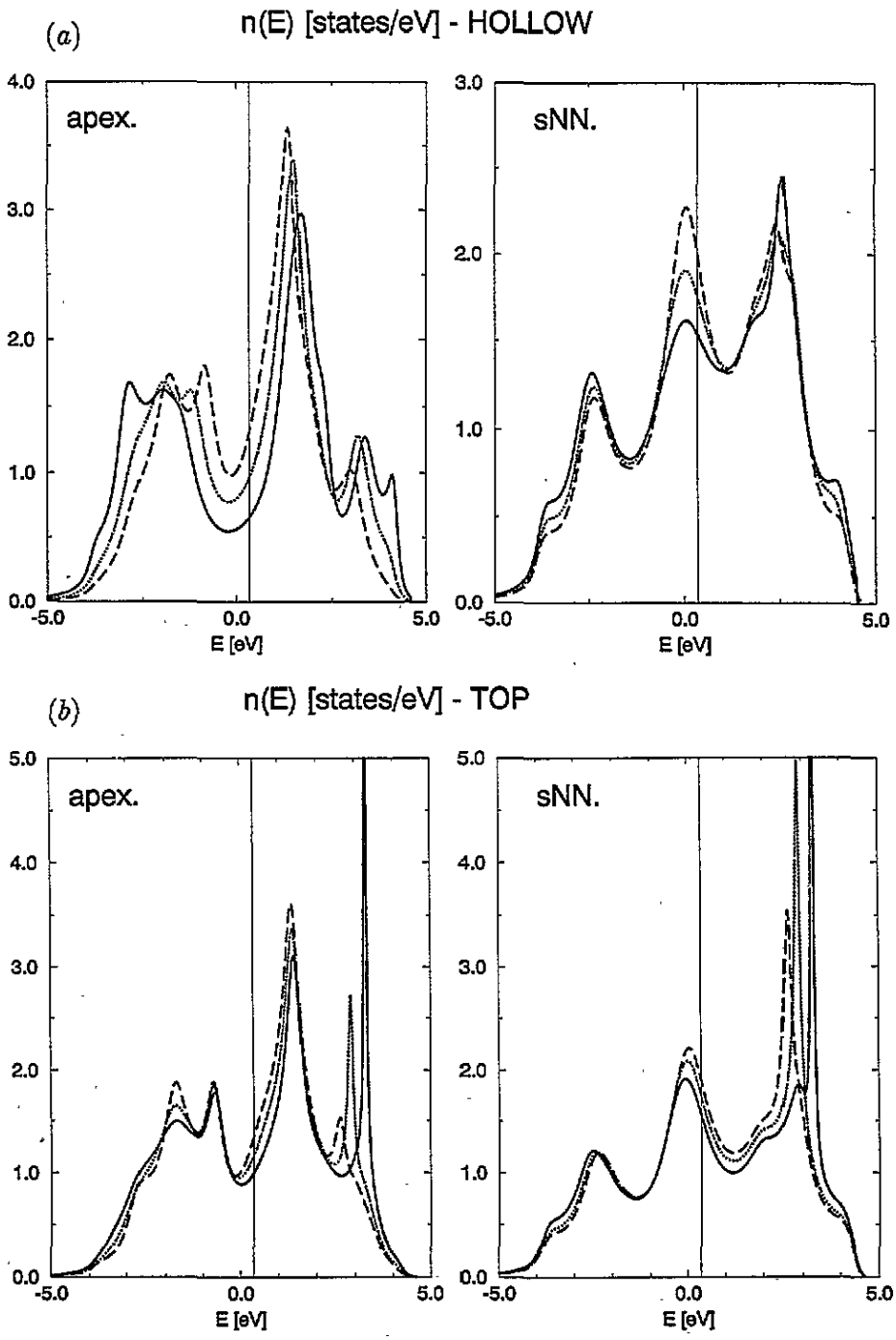

Figure 2. The LDOS of the apex and of its sample surface NN (sNN) for different values of the T/S separation. d is the perpendicular distance between the apex and the sample surface. (*a*) Hollow site. The full line is for $d/d_{(001)} = 1.1$, the dotted line for $d/d_{(001)} = 1.4$ and the dashed line for $d/d_{(001)} = 2.0$. (*b*) Top site. The full line is for $d/d_{(001)} = 1.6$, the dotted for $d/d_{(001)} = 1.8$ and the dashed for $d/d_{(001)} = 2.0$. The energies are given in electron volts, the values of the densities of states are given in states per electron volt and the vertical line represents the Fermi level ε_F.

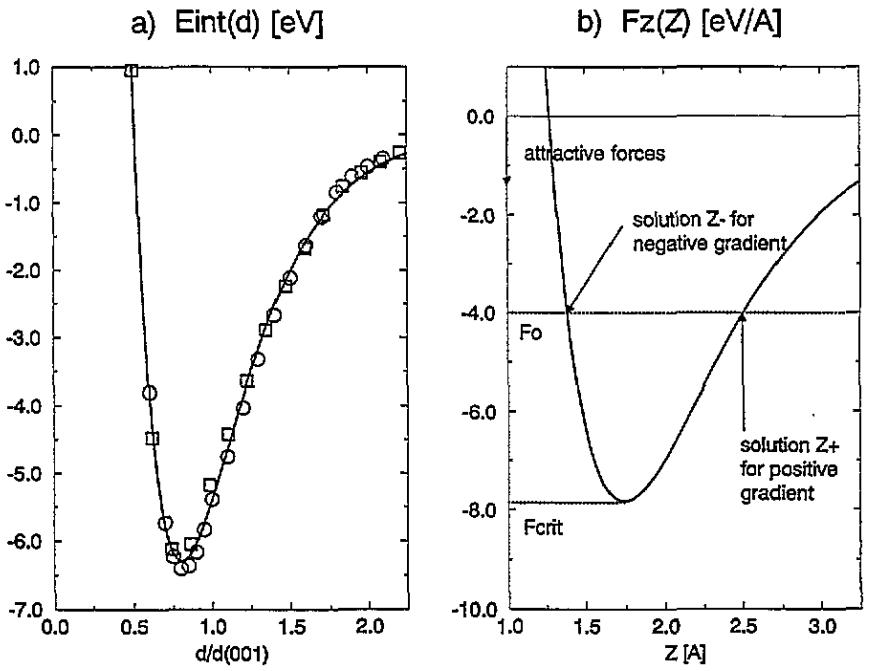

Figure 3. (*a*) Interaction energies E_{int} between pyr(001) $h = 4$ and W(001) for a hollow site. They are obtained with the constant-LDOS model (squares) and with the complete electronic structure calculation (circles). The full line is the corresponding Rydberg function. (*b*) A schematic representation of the force $F_z(r, z)$ for a given r value and definitions used in the text for solving the equation $F_z(r, z) = F_0$.

One finds the same trends for the sNN LDOS (figure 2(*b*)). The peak located above ε_F is also shifted towards the top of the band, with an increasing amplitude, for decreasing values of d. This peak originates also mainly from the d_{z^2} orbital of the sNN. The positions of these peaks (for the three values of d, i.e. $d/d_{(001)} = 1.6, 1.8, 2.0$) correspond exactly to those of the aLDOS peaks.

We have shown that strong modifications of the LDOS happen for tip and sample atoms interacting directly via non-zero hopping integrals. These modifications are sensitive to small variations of d and to the nature of the site facing the apex. They are due to the strong T/S interaction which occurs in the intermediate regime ($1 \leqslant d/d_{(001)} \leqslant 2$ for (001) planes) for which a 'chemical' bonding appears between the tip and the sample atoms. This 'strong' interaction is characterized by the tip-induced localized states (TILS) previously introduced by Ciraci *et al* [8]. Such states 'are formed from the bonding and antibonding combination of tip and sample states' [8] and lead to the LDOS modifications described above.

This study shows again that the T/S interactions modify strongly the LDOS, so that the tunnelling current between the tip and the sample cannot be calculated in the intermediate regime we consider here from the free apex and sample surface LDOS [34].

4. T/S interaction energy

The T/S interaction energy $E_{int}(d)$ is determined by the total energy difference between the coupled and uncoupled systems versus the T/S distance d.

4.1. Properties of the T/S interaction energy

The T/S interaction energy $E_{int}(d)$, which is obtained by integrating the LDOS [1], is much less sensitive to the modifications of the local environment than the LDOS themselves. This is why E_{int} is mostly given by the local energies of the most perturbed atoms, i.e. by those tip and sample atoms which are directly coupled by non-zero hopping integrals. A previous work [35] shows that most of the interaction energy originates from these atoms, even if the others can contribute significantly (up to 20%) to the total interaction energy (see table 1 in [35]). Therefore E_{int} is nearly insensitive to the tip's morphology *only* if such strongly coupled atoms remain the same.

Moreover, it has been previously suggested that, while the magnitude of the interaction energy is sensitive to the tip's morphology and to the tip material, the interaction energy versus d curve has 'universal' form independently of these parameters [36]. We have verified that the curves we obtain for $E_{int}(d)$ satisfy this scaling law and can be written as $E_{int}(d) = \Delta E f(d-d_0)/L$. ΔE is the maximum interaction energy, d_0 is the separation at which this maximum occurs and L is related to the curvature of this maximum. Moreover $f(u)$ fits, rather well, to the Rydberg function given in [36] *when and only when* the tip is facing high-symmetry surface sites. Note that the values of ΔE, d_0 and L are strongly sensitive to the considered site: $\Delta E(d_0)$ are (respectively) much larger (smaller) for the hollow (top) site, the T/S interaction occurring via a larger (smaller) number of T/S bonds.

4.2. Friedel's model for the LDOS and T/S interaction energy

The detailed calculations of the LDOS are not necessary to obtain the *general trends* for transition metal cohesive or surface energies [37, 38]. It is often sufficient to assume that the LDOS is constant (Friedel's model [37]), the width of the square LDOS being fitted to its exact tight-binding value. We have verified [35] that the T/S interaction energy can also be obtained with a good accuracy using this simple assumption. For example, compare the interaction energies between a perfect pyr(001) $h = 4$ facing an H site of a W(001) surface (figure 3(*a*)). These energies are obtained both with the simple constant-LDOS model and with the 'exact' electronic structure calculations.

Even if the energies obtained with the two methods of calculation are not strictly equal for all d values, the qualitative trends remain the same for both calculations. In order to quantify the differences between these two methods, one can compare the relative evolution of the interaction energy between the H site and the T site. For that, we characterize the contrast by the quantity $C(d)$ defined by $C(d) = (E_{int}^{HOLLOW} - E_{int}^{TOP})/(E_{int}^{HOLLOW} + E_{int}^{TOP})$. The results obtained with the two methods of calculation are very close to each other (figure 4). Note that the divergence observed in the $C(d)$ curve is due to the fact that the sum $E_{int}^{HOLLOW} + E_{int}^{TOP}$ is zero for this d value. This shows that AFM images with a satisfactory contrast can be calculated within the constant-LDOS model.

Finally, note that the magnitude of E_{int} i.e. the scaling factor ΔE (i) depends sensitively on the tip and sample material (via the band width and the band filling) and varies as the cohesive energy with the band filling and (ii) is qualitatively identical for both A tip/B sample and B tip/A sample (see figure 1(*b*) [39]).

5. AFM images

The approximation of constant LDOS, which is also called the second-moment approximation, allows us to obtain the interaction energies within short computing times.

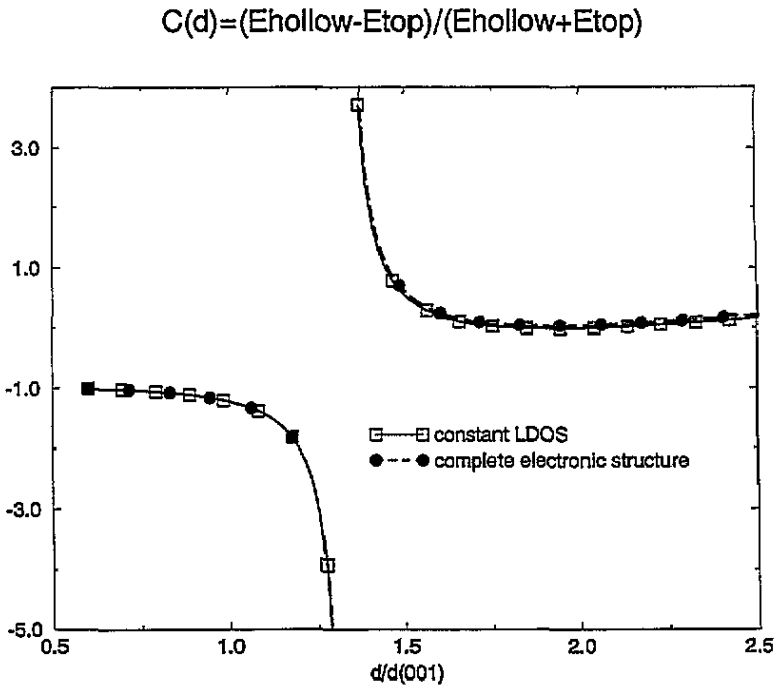

Figure 4. Contrast $C(d) = (E_{int}^{HOLLOW} - E_{int}^{TOP})/(E_{int}^{HOLLOW} + E_{int}^{TOP})$ versus d (the same notation as in figure 3(*a*)).

This is why we use it to simulate AFM images when the tip scans the sample surface and for various tip morphologies, sample surfaces with or without steps, deposited clusters, etc. The next section is devoted to the method of calculation and to the results obtained from this study.

5.1. Model for the energy

In this scheme, the local energies E_i of the atoms i result from an attractive band energy E_{bi} contribution and from a repulsive energy E_{ri} contribution. E_{bi} is calculated from

$$E_{bi} = (N-10)N/20 \sqrt{\sum_{j \neq i}^{R_{ij} < R_c} t^2(R_{ij})}$$

where N is the band filling of the 'd' bands. The hopping integrals $t(R_{ij})$ are now assumed to decay continuously with interatomic distances R_{ij} down to zero for the fifth NNs ($R_c = R_5$), with a hyperbolic cosine analytical form, R_{ij} being the distance between atom i and atom j.

The repulsive energy contribution E_{ri} is described by a pair potential:

$$E_{ri} = A_r \sum_{j \neq i}^{R_{ij} < R_c} f_r(R_{ij})$$

for simplicity, the $f_r(R)$ function having the same analytical form as the $t(R)$ function. We have chosen these continuous decaying $t(R)$ and $f_r(R)$ functions to avoid discontinuities of the total energy derivatives. The repulsive parameters are fitted as previously to obtain the

experimental values for the lattice parameter, the isotropic compressibility and the cohesive energy of tungsten [1].

5.2. Tip/sample interaction

The AFM images are obtained from the T/S interaction energies. They are determined by the total energy difference between the coupled and uncoupled systems versus d and for a set of different tip positions $r = (x, y)$ over the sample surface (S): $E_{int}(r, d) - E(r, \infty)$.

The W tips we consider are the same as above (see subsection 2.3). They are built up from $h = 8, 9$ bcc(001), (111) planes respectively. We also study the effects of truncated tips with multiatomic apexes with $n = 9$ atoms for (001) planes, 3 or 6 atoms for (111) planes (noted tpyr(hkl) n apex atom(s) with (hkl)= (001) or (111)). The sample surface (S) is assumed to be a perfect semi-infinite bcc crystal, limited by a surface with or without steps. Adsorbates or clusters can also be deposited on its surface. The (S) and (TSp) surface lattice vectors are tilted by an angle θ (figure 5).

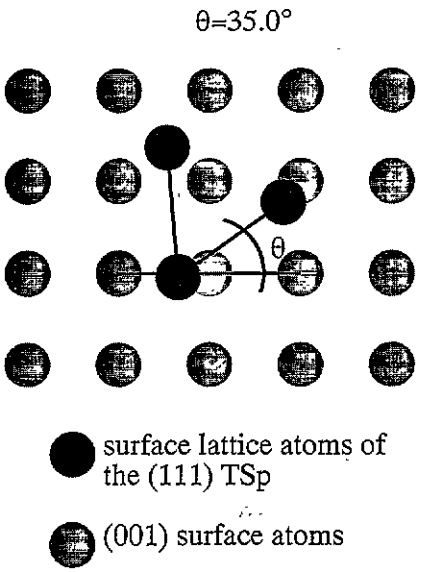

Figure 5. The definition of the tilt angle θ between the surface lattice vectors of a (111) TSp and those of a (001) sample surface.

The present study is devoted to the influence of the tip's morphology on the contrast of AFM images. We guess that in the attractive force regime we essentially consider here, the approximation of rigid T/S does not change the qualitative features we obtain for the contrast (see subsection 2.3).

In this first study, we are only interested in the perpendicular component of the force defined by $F_z = -\mathrm{d}E_{int}(r, z)/\mathrm{d}z$ for a fixed r (the z axis being perpendicular to the (S) and (TSp) surfaces, even if the crystallographic orientations of these surfaces are different). We have calculated images either in the constant-force or in the constant-z mode. For a constant force $F_z = F_0$, the tip follows an interaction surface $Z_{F_0}(x, y)$ which is usually taken to be the surface topography.

We are especially interested in the attractive regime ($F_0 < 0$). In this case, for each r there exist two Z solutions (Z_- and Z_+) satisfying the equation $F_z(r, z) = F_0$. They are characterized respectively by a negative and by a positive force gradient (see figure 3(b)). Furthermore, the equation cannot be solved for force values smaller than the critical force

$F_{crit}(r)$ which is the corresponding largest attractive force. Therefore the constant-force surface $Z_{F_0}(x, y)$ can only be obtained in a limited range of attractive forces. Within this range, the $F_z(r, z) = F_0$ equation can be solved for all the r positions of the tip over the sample's surface and for the same force gradient sign. The lower boundary F_L of the attractive force range is defined by the value $F_L = F_{crit}(r_b)$ for a specific tip position r_b for which $F_{crit}(r_b) \geqslant F_{crit}(r)$, $\forall r$.

In the images we present here, the $x(y)$ axis is represented by the horizontal (vertical) axis (respectively). From the constant-force surface $Z_{F_0}(x, y)$, we define the corrugation ΔZ as $\Delta Z = Z_{F_0}\max - Z_{F_0}\min$ and the average T/S separation as $Z_m = (Z_{F_0}\max + Z_{F_0}\min)/2$.

In the following, we consider a perfect W(001) surface, a surface with a monoatomic step and finally a W(001) surface on which clusters are deposited.

5.3. Images of a perfect W(001) surface

Let us summarize the main results we obtain for perfect surfaces [39]. Using monatomic apex tips, the images have the right periodicity of the sample surface lattice and the maxima of the $Z_{F_0}(x, y)$ surface correspond to the real atomic positions. In the constant-force mode, a larger corrugation is observed for the (001) tip than for the (111) tip: $\Delta Z(001) = 1.49$ Å, $\Delta Z(111) = 1.14$ Å for a force $F_0 = -1.0$ eV Å^{-1} with a negative gradient ($Z_m \approx 1.98$ Å). As expected the corrugation decreases when the T/S distance increases: $\Delta Z(001) = 0.19$ Å, $\Delta Z(111) = 0.13$ Å for a force $F_0 = -1.0$ eV Å^{-1} with a positive gradient ($Z_m \approx 3.10$ Å).

For truncated tips, the corrugation decreases with the number of apex atoms: for a constant force $F_0 = -1.0$ eV Å^{-1} with a positive gradient, we obtain $\Delta Z = 0.071$ Å for a tpyr(111) with three apex atoms, 0.054 Å for a typr(111) with six apex atoms and 0.058 Å for a tpyr(001) with nine apex atoms. The images, obtained with multiatomic apex tips, exhibit 'distortions' (i.e. band or zig-zag patterns, contrast inversion) which were previously reported both experimentally and theoretically in the repulsive regime [12, 39, 40]. These 'distortions' depend strongly on the tip morphology and on the θ value. The band or zig-zag patterns are mostly observed with truncated (111) tips, so that the maxima of the $Z_{F0}(x, y)$ surface do not match any longer with the real atomic positions. An example of these band patterns is given in the next section.

5.4. Images of a stepped W(001) surface

Here we consider a W(001) surface with a monatomic $(\bar{1}01)$ step. The black straight line on the images represents the $x = 0$ step's edge position. Using a perfect pyr(111), the images (figure 6(*a*)) have the right periodicity of the sample surface lattice, and the maxima correspond to the atomic positions. In order to analyse the surface corrugation and the step's height, cuts are made along the y axis, as represented by the AA′ and BB′ lines (figure 6(*b*)). The AA′ line is a line of H sites to the left of the step ($x < 0$) and a line of T sites to the right of the step (and *vice versa* for the BB′ line). Far from the step's edge, we recover the W(001) corrugation previously obtained for a perfect pyr(111) (i.e. $\Delta Z = 1.1$ Å) for $F_0 = -1$ eV Å^{-1} with a negative gradient (figure 6(*a*)). We also estimate the average step's height $\Delta Z_{step} \approx 1.6$ Å which corresponds quite well to the (001) interplanar distance ($d_{(001)} = a_0/2 = 1.58$ Å).

For an attractive force of $F_0 = -1.0$ eV Å^{-1} with a positive gradient, the average T/S distance increases as expected and the corrugation of the surfaces far from the step's edge decreases by one order of magnitude approximately (figure 6(*b*)). The surface corrugation

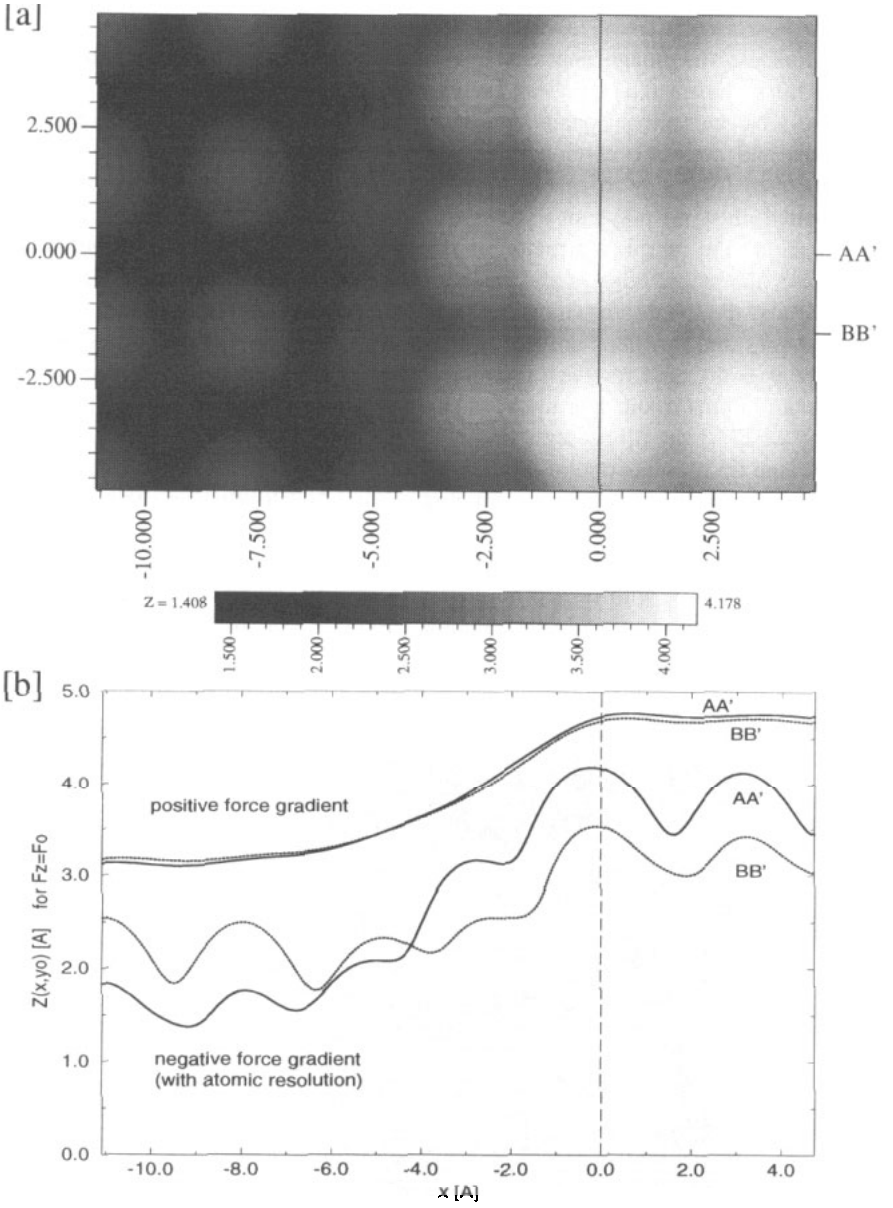

Figure 6. (*a*) A constant-force image of a W(001) surface with a monatomic step using a perfect pyr(111) tip. The value of the constant force is $F_0 = -1.0$ eV Å^{-1} with negative gradient and $\theta = 27.5°$. The lateral dimensions are $5a_0 \times 5a_0$ (with the lattice parameter $a_0 = 3.1655$ Å), and Z is given in ångströms. The vertical line represents the real $x = 0$ step's edge position. Far from the step's edge, the imaged atoms match with the real atomic positions. Note the presence of 'phantom' atoms just to the left of the step's edge. (*b*) Cuts along the AA′ and BB′ lines as defined in (*a*) for the attractive force $F_0 = -1.0$ eV Å^{-1} with both negative and positive gradient. Note that the average step's height remains the same for the different constant-force values.

is very small as compared to the step's height so the atomic resolution is practically lost. Note that we always find the same value for the step's height ($\Delta Z_{step} \approx 1.6$ Å) for all

values of F_0.

Let us now discuss the image near the left of the step's edge (bumps in the range $-3.0 < x < -2.0$ in figure 6(*a*)). These imaged 'atoms' do not correspond to sample atomic positions. **We call them 'phantom' atoms.** In fact, the AFM images are T/S interaction images and therefore contain information about both the tip and the sample. As already mentioned [39], the sharpness of the tip and (or) of the sample's structures (i.e. steps, deposited clusters) plays an important role. The role of AFM probe is played either by the tip or by the sample's structure depending on which has the sharpest shape. In the present case, the step's edge is sharper than the perfect pyr(111) itself. Hence the step's edge atoms and the 'phantom' atoms are in fact tip's atoms imaged by the step itself. Therefore their shapes and positions are strongly dependent on the tip morphology and on the θ values. For $\theta = 90°$ and for the same conditions as above, we do not observe any longer the 'phantom' atoms in the step image (figure 7). These effects can be explained by the fact that for $\theta = 27.5°$ the tip presents one of its three edges directed towards the step while for $\theta = 90°$ the tip presents one of its three faces towards the step. Consequently, for $\theta = 27.5°$, the step's edge images the tip apex and its first NN located on the tip's edge. For $\theta = 90°$, the step's edge images a part of the oriented tip's side yielding an 'average' image. We have performed calculations for other values of θ and observe that the positions of the 'phantom' atoms move with respect to the θ values. This study of a stepped surface reveals the reciprocity between tip and sharp sample structures observed in the images. An even more convincing example is given in subsection 5.5.

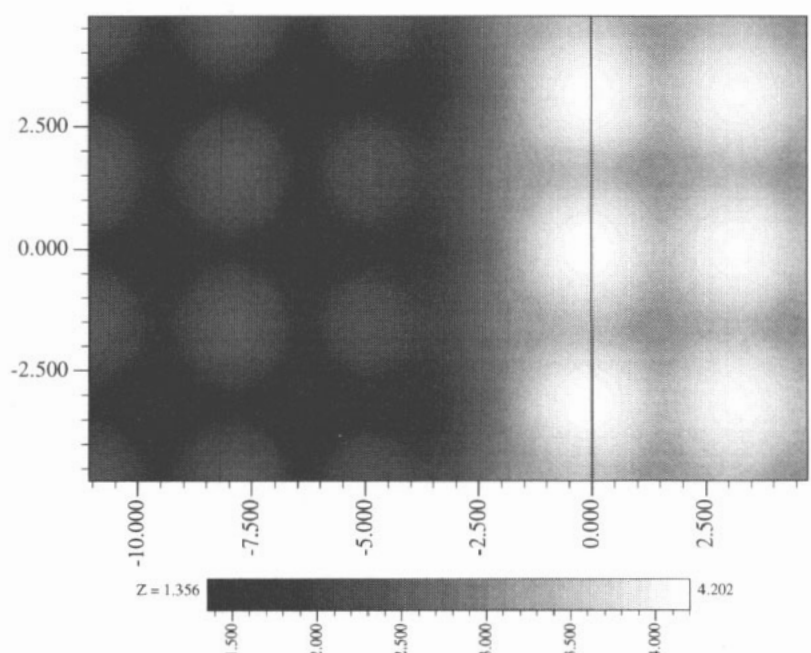

Figure 7. A constant-force image with the same conditions as in figure 6(*a*) except that now $\theta = 90°$. Note the disappearance of the 'phantom' atoms.

For truncated tips (typr(111) with three apex atoms), the corrugation on the surfaces far from the step's edge decreases with the number of apex atoms as mentioned in subsection 5.3, the average step height keeping the same value as for perfect tips (figure 8(*b*)). We

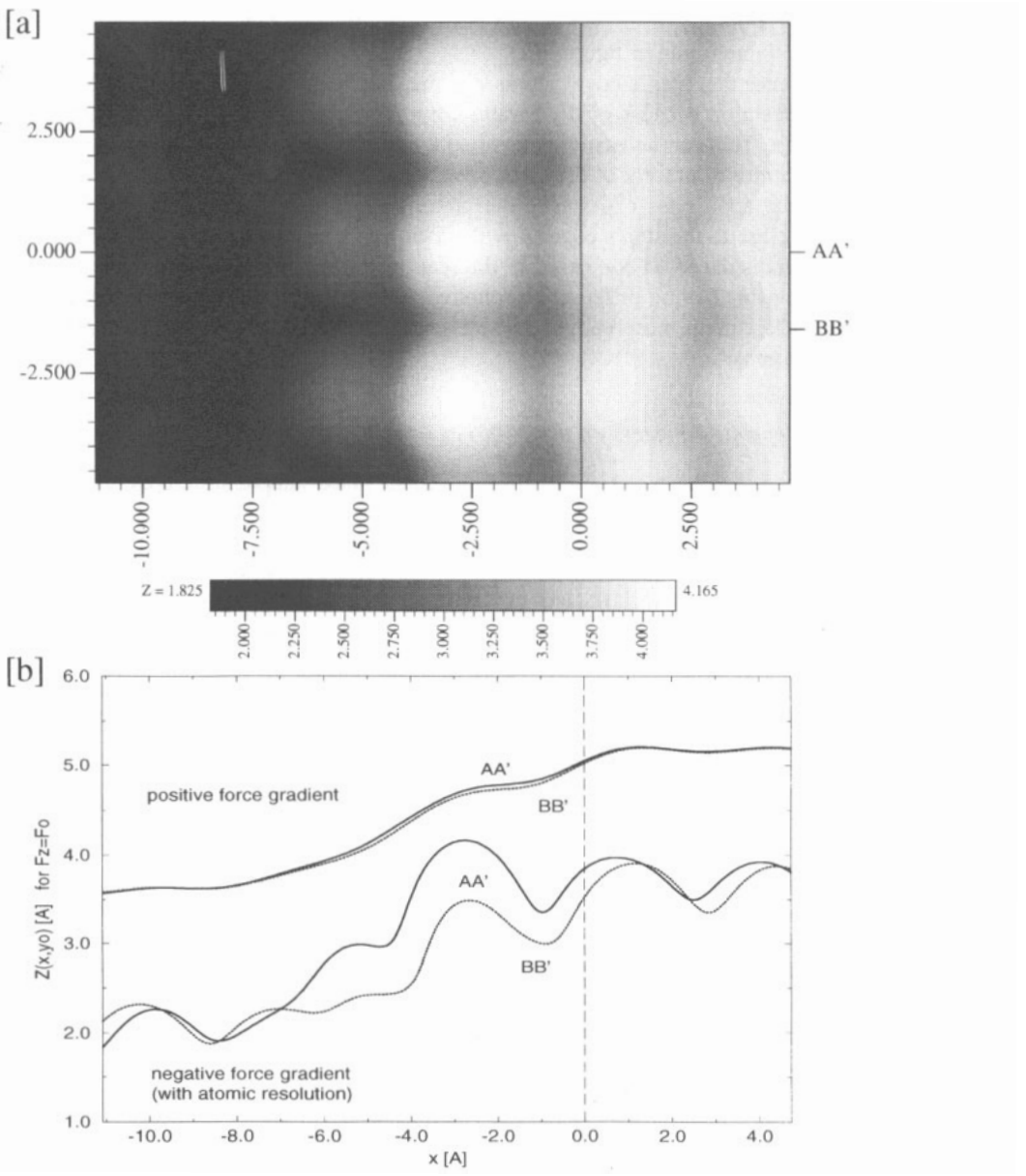

Figure 8. (*a*) A constant-force image of a W(001) surface with a monatomic step using a pyr(111) three apex-atom tip. The value of the constant force is $F_0 = -1.0$ eV Å^{-1} with negative gradient and $\theta = 27.5°$. The lateral dimensions are $5a_0 \times 5a_0$ and Z is given in ångströms. The vertical line represents the real $x = 0$ step's edge position. Note the distortions exhibited on the surfaces far from the step's edge and the displacement of the imaged step's edge with respect to the real position. (*b*) Cuts along the AA′ and BB′ lines defined in (*a*). Note that the average step height is the same as in figure 6(*b*).

also observe band patterns on the surfaces (figure 8(*a*)) which can be explained in terms of multiatomic apexes as mentioned in 5.3. This peculiar band pattern is due to the fact that one side of the triangular apex atoms lies nearly along the surface sample [010] rows

(because $\theta = 27.5°$). However, we cannot easily interpret the band shape which can be symmetric or asymmetric as in figure 8(*a*).

We also observe the 'step's edge' atoms and the 'phantom' atoms (both for the same y constant-value direction because of the θ value), but their positions are displaced to the left of the step's edge. This can be easily understood by the fact that the tip position $r = (x, y)$ is given by the centre of gravity of the three apex atoms' triangle. However some tip atoms and especially the apex ones experience the presence of the step atoms (and *vice versa*) before the tip is close to the step's edge ($x = 0$). This explains qualitatively why the imaged step's position is displaced as compared to the real position.

Finally, using tips having different morphologies, we always find the same step height, even if these different tip morphologies induce peculiar effects such as band patterns and (or) 'phantom' atoms.

5.5. Images of deposited clusters on the W(001) surface

In order to really show the reciprocity between tip and sharp sample structures, we present some images of deposited clusters. The cluster supported by the W(001) surface is represented by a five-atom pyramid with a square base. The cluster's edge angle, with respect to the z axis, is smaller than the edge angle of pyr(111) tips, i.e. it is sharper than the pyr(111) tips. The image of this cluster, obtained for a tpyr(111) with three apex atoms (for a constant force $F_0 = -1.0$ eV Å^{-1} with a negative gradient), is shown in figure 9. In fact, we do not observe the cluster which has a fourfold symmetry, but rather the first tip planes with a threefold symmetry. As already mentioned, the images originate from T/S interaction and contain information about both the tip and the sample. In the case we consider here, the sample's structure, i.e. the deposited cluster, is sharper than the tip itself and plays, in fact, the role of the probe. This is why the cluster 'images' the topmost atoms of the tip, the number of imaged tip planes being directly related to the cluster's height. Note that, around this feature, one finds again the W(001) surface image, which exhibits distortions (band patterns) because of the multiatomic apex effects.

Note that we have presented an image with a negative force gradient because the atomic resolution is obtained with these forces. For attractive forces with negative gradient, the atomic resolution is lost as observed above (figure 6(*b*), section 4) but we also observe a 'cluster' with a threefold symmetry for a constant force $F_0 = -1.0$ eV Å^{-1} with a positive gradient.

In order to emphasize the relative role of the tips and sharp clusters, the deposited cluster is now flattened so that its edge angle is equal to that of the pyr(111) tip. The image, obtained for a tpyr(111) with three apex atoms and a constant force $F_0 = -0.3$ eV Å^{-1} with a negative gradient, exhibits a peculiar effect (figure 10). One can observe the threefold symmetry of the multiatomic apex, but the cluster's fourfold symmetry is also found around each imaged apex atoms. Note that, now, we only image the first two 'tip planes' because the cluster has been flattened.

This example illustrates clearly the problems encountered in the interpretation of T/S interaction images and the respective roles played by the tips and sharp deposited clusters.

5.6. Can atomic resolution be obtained experimentally?

Let us now discuss the conditions to obtain images with atomic resolution. We have shown that the atomic resolution can be achieved on a perfect W(001) surface for attractive forces with both negative or positive gradients. Qualitatively, for monatomic apex tips

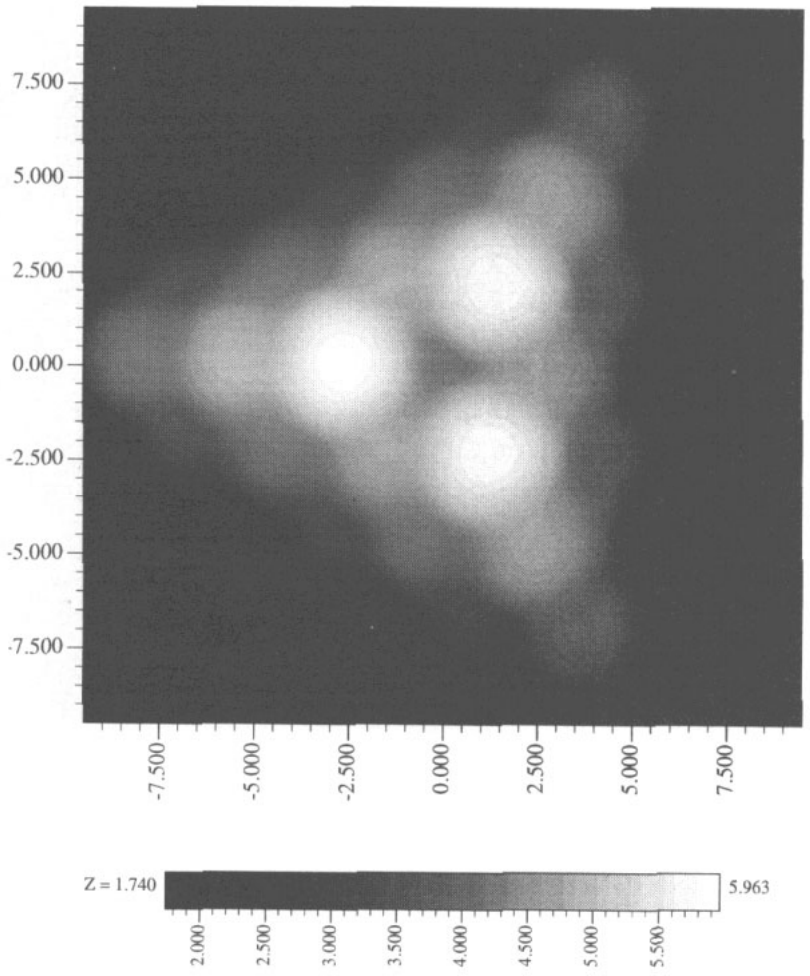

Figure 9. A constant-force image of a W(001) surface with an adsorbed cluster (five-atom pyramid) using a W(111) three-apex-atom tip ($F_0 = -1.0$ eV Å^{-1} with negative gradient and $\theta = 27.5°$). The lateral dimensions are $6a_0 \times 6a_0$ and Z is given in ångströms.

the calculated surface corrugation is in the ångström range for negative force gradient and decreases by approximately one order of magnitude for corresponding forces with positive gradient. The corrugation is much smaller when considering multiatomic apex tips. However, for surfaces with defects (steps or deposited clusters), atomic resolution is only obtained for attractive forces with a negative gradient, because in such cases the surface corrugation is of the same order of magnitude as the 'defect corrugation' (at least for the cases we have considered). For attractive forces with a positive gradient, the surface corrugation is one order of magnitude smaller then the step or cluster's height. Therefore the atomic resolution is lost in the corresponding images (for example see figure 6(*b*), and figure 4(*b*) in [39]).

Experimentally force measurements can be performed using two different techniques. (i) In static measurements, the force is deduced from the deflection of the cantilever multiplied by the spring constant k of the tip/cantilever system. Nevertheless, cantilever instabilities occur when the gradient of the considered $F_z(r, z)$ force exceeds the value of the spring

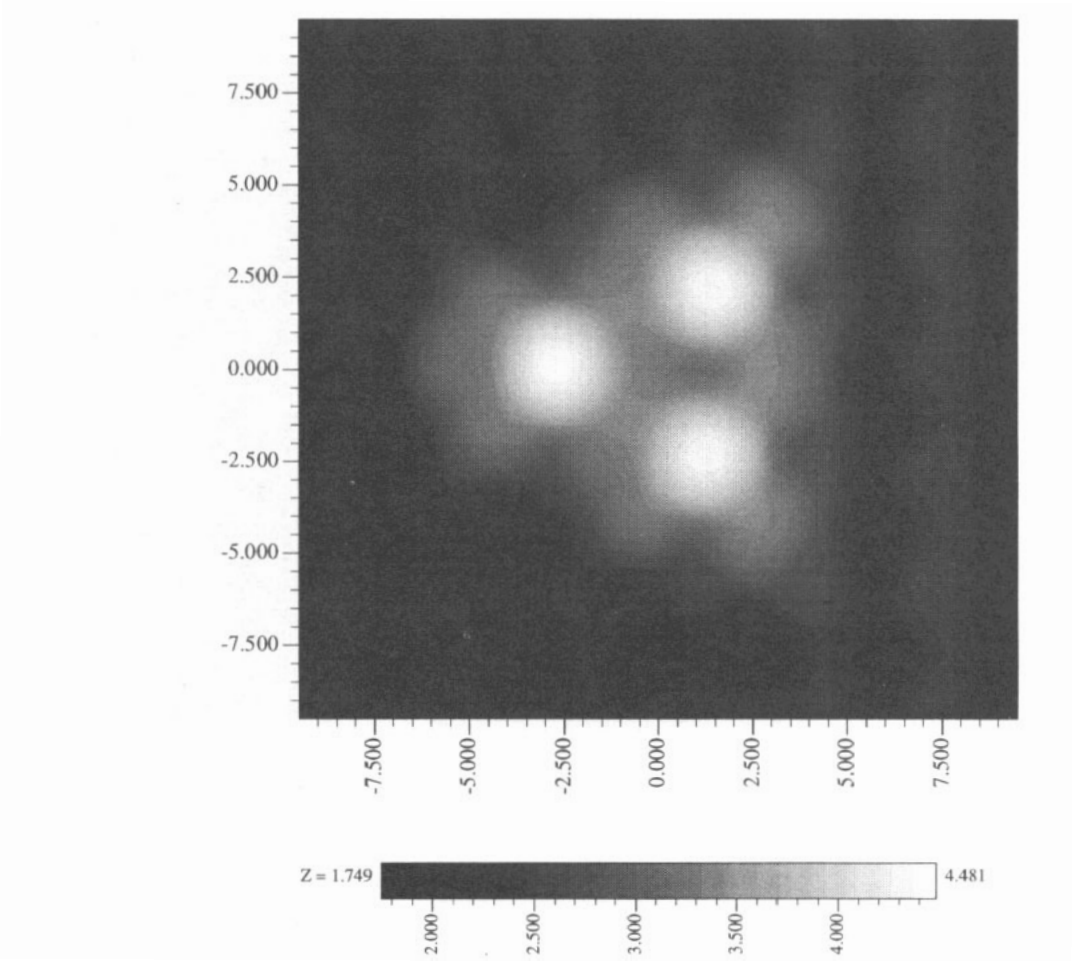

Figure 10. A constant-force image of a W(001) surface with a flattened adsorbed cluster using a W(111) three-apex-atom tip ($F_0 = -0.3$ eV Å^{-1} with negative gradient and $\theta = 27.5°$). The lateral dimensions are $6a_0 \times 6a_0$ and Z is given in ångströms. Note the fourfold symmetry of the cluster around each imaged apex atom.

constant k. It can be shown that these instabilities *always* occur within the positive force gradient range. (ii) Dynamic measurements such as those performed by Dürig *et al* [17] rely on the shift of the cantilever's resonance frequency induced by the T/S interaction. This frequency shift is related to the corresponding T/S force gradient. However for negative force gradients, the sign of the forces (i.e. repulsive or attractive forces) can only be known by integrating the force gradients.

It is expected that atomic resolutions can be obtained in the attractive force regime with a negative gradient. However the fundamental experimental problems are the *a priori* choice (i) of the spring constant k, which has to be sufficiently large to avoid tip/cantilever instabilities but not too large to be sensitive enough to 'small' T/S interaction forces, and more especially (ii) of the constant force F_0 which has to be measured for any tip positions $\boldsymbol{r}$ during the surface scans.

6. Conclusion

In this paper, we have investigated the electronic structure of transition metal nanotips with different morphologies interacting with transition metal surfaces. We used the tight-binding approximation in order to describe the band structure of the considered tips and samples and we determined the LDOS from the real space recursion method.

We have studied the interaction of W supported nanotips with a W(001) surface within the intermediate-interaction regime (i.e. $d = 2$–5 Å). The main results can be summarized as follows. (i) The LDOS of the apex and of its surface NN change drastically with the T/S separation distance d. The observation of a strong hole in the middle of the band or of new peaks occurring from strong directed T/S bonds depends on the nature of the surface site facing the tip (H site or T site). (ii) These LDOS modifications have been explained in terms of TILS, which were introduced by Ciraci *et al* [8]. They have also to be taken into account when performing a tunnelling current calculation, at least for the T/S distance we consider here. (iii) The T/S interaction energy curves follow a scaling law, as a first approximation, when and only when the tip's apex is above high-symmetry sample sites. These energetic properties could be obtained with a good accuracy by assuming that the LDOS are constant (Friedel's model). This approximation reduces considerably the computing times for the interaction energies. (iv) Finally within the model of a square LDOS, we have obtained AFM images especially for transition metal tips and samples and for the interaction range dominated by adhesion-type forces. The study of W(001) surfaces has revealed that the 'flatter' the tip is, the smaller the corrugation is. The role of the AFM probe can be played either by the tip or by surface sample 'structures' (i.e. step edges, deposited clusters) depending upon their relative sharpness. With truncated tips, distorted images are obtained as already observed both experimentally and theoretically. The conditions to obtain atomic resolution are also discussed.

The range of validity of the calculations we present here is limited by (i) the neglect of the deformations resulting from the T/S interactions and (ii) the use of a semiempirical method. The first assumption restricts the range of T/S distances for which the calculations can be considered to be realistic. Tight-binding molecular dynamics calculations are now under progress in order to take account of these effects. On the other hand, the use of semiempirical methods to study such effects is required, at least for transition-metal-based systems, by the large number of inequivalent atoms and the large computing times needed to obtain images with a reasonable accuracy. However considering the recent progress of the Car–Parrinello method [41] combined with 'appropriate' pseudopotentials for transition metals [42,43], an *ab initio* calculation of the interaction for such systems is expected to be possible in the near future. Note finally that we considered here, for simplicity, non-magnetic systems. The magnetic interaction between transition metal tips and samples is now being studied and will be presented in a forthcoming paper.

Acknowledgments

We wish to acknowledge D Stoeffler for fruitful discussions and critical comments concerning the numerical results obtained in this study.

References

[1] Ness H and Gautier F 1995 *J. Phys.: Condens. Matter* **7** 6625–40
[2] Bardeen J 1961 *Phys. Rev. Lett.* **6** 57
[3] Tersoff J and Hamann D R 1985 *Phys. Rev.* B **31** 805
[4] Tsukada M and Shima N 1987 *J. Phys. Soc. Japan* **56** 2875
[5] Chen C J 1990 *Phys. Rev.* B **42** 8841
[6] Sacks W and Noguera C 1991 *Phys. Rev.* B **43** 11 612
[7] Tekman E and Ciraci S 1989 *Phys. Rev.* B **40** 10 286
[8] Ciraci S, Baratoff A and Batra I P 1990 *Phys. Rev.* B **41** 2763
[9] Doyen G, Drakova D and Scheffler M 1993 *Phys. Rev.* B **47** 9778
[10] Binnig G, Quate C F and Gerber Ch *1986 Phys. Rev. Lett.* **56** 930
[11] Dürig U, Gimzewski J K and Pohl D W 1986 *Phys. Rev. Lett.* **57** 2403
[12] Binnig G, Gerber Ch, Stoll E, Albrecht T R and Quate C F 1987 *Europhys. Lett.* **3** 1281; 1987 *Surface Sci.* **198/190** 1
Marti O, Drake B and Hansma P K 1987 *Appl. Phys. Lett.* **51** 484
Marti O, Drake B, Gould S and Hansma P K 1988 *J. Vac. Sci. Technol.* A **6** 287
[13] Albrecht T R and Quate C F 1987 *J. Appl. Phys.* **62** 2599; 1988 *J. Vac. Sci. Technol.* A **6** 271
[14] Meyer E, Anselmetti D, Wiesendanger R, Güntherodt H J, Levy F and Berger H 1989 *Europhys. Lett.* **9** 695
[15] Meyer E, Heinzelmann H, Rudin H and Güntherodt H J 1990 Z. *Phys.* B **79** 3
Meyer G and Amer N M 1990 *Appl. Phys. Lett.* **56** 2100
[16] Manne S, Butt H J, Gould S and Hansma P K 1990 *Appl. Phys. Lett.* **56** 1758
Manne S, Hansma P K, Massie J, Elings V B and Gewirth A A 1991 *Science* **251** 184
[17] Dürig U and Züger O 1993 *Nanostructures and Manipulation of Atoms Under High Fields and Temperatures: Applications (NATO ASI Series E: Applied Sciences)* vol 235, V T Binh, N Garcia and K Dronsfeld (Dordrecht: Kluwer) p 271
Dürig U, Züger O and Stalder A 1992 *J. Appl. Phys.* **72** 1778
Dürig U, Züger O and Pohl D W 1990 *Phys. Rev. Lett.* **65** 349
[18] Zhong W, Overney G and Tomanek D 1991 *Phys. Rev. Lett.* **15** 49
[19] Ciraci S, Baratoff A and Batra I P 1990 *Phys. Rev.* B **42** 7618
[20] Ciraci S, Tekman E, Baratoff A and Batra I P 1992 *Phys. Rev.* B **46** 10 411
[21] Abraham F, Batra I P and Ciraci S 1988 *Phys. Rev. Lett.* **60** 1314
[22] Tekman E and Ciraci S 1991 *J. Phys.: Condens. Matter* **3** 2613
[23] Bozzolo G and Ferrante J 1992 *Ultramicroscopy* **42–44** 55
[24] Landman U, Luedtke W D, Burnham N A and Colton R J 1990 Science **248** 454
[25] Sutton A P, Pethica J B, Rafii-Tabar H and Nieminen J A 1992 *Electron Theory in Alloy Design* ed D G Pettifor and A H Cottrell (London: Institute of Materials) p 191
[26] Binh V T and Garcia N 1991 *J. Physique I* **1** 605
Binh V T, Purcell S T, Garcia N and Doglioni J 1992 *Phys. Rev. Lett.* **69** 2527
Garcia N, Vu Thien Binh and Purcell S T 1993 *Surf. Sci. Lett.* **293** L884
[27] Treglia G, Desjonquères M C and Spanjaard D 1983 *J. Phys. C: Solid State Phys.* **16** 2407
[28] Gschneidner K A 1964 *Solid State Physics* vol 16 (New York: Academic) p 275
[29] Slater J C and Koster G F 1954 *Phys. Rev.* **94** 1498
[30] Haydock R 1980 *Solid State Physics* vol 35 (New York: Academic) p 215
[31] Beer N and Pettifor D G 1984 *The Electronic Structure of Complex Systems* ed P Phariseau and W M Temmerman (New York: Plenum) p 769
[32] Pethica J B and Sutton A P 1988 *J. Vac. Sci. Technol.* A **6** 2490
[33] Pizzagalli L, Bouette S, Stoeffler D, Gautier F to be published
[34] Ohnishi S and Tsukada M 1989 *Solid State Commun.* **71** 391
[35] Gautier F, Ness H and Stoeffler D 1992 *Ultramicroscopy* **42–44** 91
[36] Banerjea A, Smith J R and Ferrante J 1990 *J. Phys.: Condens. Matter* **2** 8841 and references therein
[37] Friedel J 1969 *The Physics of Metals* ed J M Ziman (Cambridge: Cambridge University Press) p 494
[38] Desjonquères M C and Spanjaard D 1993 *Concepts in Surface Physics (Springer Series in Surface Science 30)* ed R Gomer (Berlin: Springer) p 218
[39] Ness H, Stoeffler D and Gautier F 1993 *Surf. Sci. Lett.* **294** L969
[40] Abraham F and Batra I P 1989 *Surf. Sci.* **209** L125
[41] Car R and Parrinello M 1985 *Phys. Rev. Lett.* **55** 2471; 1988 *Simple Molecular Systems at Very High Density* ed A Polian (New York: Plenum) p 455

Remler D K and Madden P A 1990 *Mol. Phys.* **70** 921
Galli G and Pasquarello A 1993 *Computer Simulation in Chemical Physics* ed M P Allen (Deventer: Kluwer) p 261
[42] Bloechl P E 1994 *Phys. Rev.* B **50** 17 953
[43] Vanderbilt D 1990 *Phys. Rev.* B **41** 7892